The Astrophysical Journal, 984:152 (9pp), 2025 May 9 https://doi.org/10.3847/1538-4357/adc380

Detection of the White Dwarf Spin of the Long-orbital Period Magnetic Cataclysmic Variable V1082 Sgr

I. J. Lima[1,2,3,4], G. Tovmassian[5,6], C. V. Rodrigues[7], A. S. Oliveira[8], G. J. M. Luna[9,10], D. A. H. Buckley[11,12,13], K. M. G. Silva[14], A. C. Mattiuci[7], D. C. Souza[8], W. Schlindwein[7], F. Falkenberg[7], and M. S. Palhares[8]

[1] Universidade Estadual Paulista "Júlio de Mesquita Filho," UNESP, Campus of Guaratinguetá, Av. Dr. Ariberto Pereira da Cunha, 333 - Pedregulho, Guaratinguetá - SP, 12516-410, Brazil
[2] CONICET-Universidad de Buenos Aires, Instituto de Astronomía y Física del Espacio (IAFE), Av. Inte. Güiraldes 2620, C1428ZAA, Buenos Aires, Argentina
[3] Universidad Nacional de San Juan, Facultad de Ciencias Exactas, Físicas y Naturales, Av. Ignacio de la Roza 590 (O), Complejo Universitario "Islas Malvinas," Rivadavia, J5402DCS, San Juan, Argentina
[4] Laboratório Nacional de Astrofísica (LNA), Rua dos Estados Unidos 154, Bairro das Nações, Itajubá, 37504-364, MG, Brazil
[5] Institute of Astronomy, Universidad Nacional Autonoma de Mexico, Ensenada, Baja California, Mexico
[6] INAF—Osservatorio Astronomico di Brera, Via E. Bianchi 46, 23807 Merate (LC), Italy
[7] Instituto Nacional de Pesquisas Espaciais (INPE/MCTI), Av. dos Astronautas, 1758, São José dos Campos, SP, Brazil
[8] IP&D, Universidade do Vale do Paraíba, 12244-000, São José dos Campos, SP, Brazil
[9] Universidad Nacional de Hurlingham (UNAHUR). Secretaría de Investigación, Av. Gdor. Vergara 2222, Villa Tesei, Buenos Aires, Argentina
[10] Consejo Nacional de Investigaciones Científicas y Técnicas (CONICET)
[11] South African Astronomical Observatory, PO Box 9, Observatory 7935, Cape Town, South Africa
[12] Department of Physics, University of the Free State, PO Box 339, Bloemfontein 9300, South Africa
[13] Department of Astronomy, University of Cape Town, Private Bag X3, Rondebosch 7701, South Africa
[14] Gemini Observatory/NSF's NOIRLab, Casilla 603, La Serena, Chile
Received 2024 December 7; revised 2025 February 19; accepted 2025 March 6; published 2025 May 7

Abstract

We report on the discovery of circular polarization modulated with a period of 1.943 ± 0.002 hr in the cataclysmic variable V1082 Sgr. These findings unambiguously reveal the rotation of a magnetic white dwarf and establish its intermediate polar nature. Along with its extraordinary long orbital period ($P_{\rm orb}$) of 20.8 hr, the spin period ($P_{\rm spin}$) places this system in an extreme position of the $P_{\rm spin}$ versus $P_{\rm orb}$ distribution. The circular polarization phase diagram has a single peak and an amplitude smaller than 1%. These data were used to model the postshock region of the accretion flow on the white dwarf surface using the CYCLOPS code. We obtained a magnetic field in the white dwarf pole of 11 MG and a magnetospheric radius consistent with the coupling region at around 2–3 white dwarf radii. The $P_{\rm spin}/P_{\rm orb}$ value and the estimated magnetic field momentum suggest that V1082 Sgr could be out of spin equilibrium or in a spin-up state, possibly in a stream accretion mode.

Unified Astronomy Thesaurus concepts: Close binary stars (254); Cataclysmic variable stars (203); Starlight polarization (1571); White dwarf stars (1799); Stellar magnetic fields (1610); Stellar accretion (1578)

Materials only available in the online version of record: data behind figure

1. Introduction

V1082 Sgr is a cataclysmic variable (CV) with an unusually long orbital period, $P_{\rm orb}$, of 20.82 hr and a complex photometric variability (D. Cieslinski et al. 1998; J. R. Thorstensen et al. 2010; F. Bernardini et al. 2013; G. Tovmassian et al. 2016). $P_{\rm orb}$ was determined from radial velocity modulation of the absorption lines from a K-type secondary star (J. R. Thorstensen et al. 2010; G. Tovmassian et al. 2016, 2018a). $P_{\rm orb}$ is also detected in photometry when the system is in the deep low state (G. Tovmassian et al. 2018b, using Kepler K2 data). The system features strong single-peaked emission lines of hydrogen and helium, except when it is in a short-lived very low state, when no emission line is detected. In the last years, mounting observational evidence points to the presence of a magnetic white dwarf (WD). A strong He II λ4686 emission line and hard X-ray emission, typical of magnetic CVs, have been reported by D. Cieslinski et al. (1998), J. R. Thorstensen et al. (2010), and J. Tueller et al. (2010). In this regard, F. Bernardini et al. (2013) detected a transient modulation with a timescale of about 2 hr in the XMM-Newton X-ray light curve. Given its transient nature, they discarded its relation with the WD spin and associated it with the mass-transfer mechanism. Their X-ray spectrum is consistent with a multitemperature optically thin thermal plasma, often found in magnetic CVs. The object is highly variable in optical, UV, and X-ray bands and is mostly irregular, showing some unstable periodic or cyclical variations on different timescales. A quasiperiodic photometric variability of about 29 days, probably associated with variations in the accretion rate, was detected by G. Tovmassian et al. (2016, 2018b).

There are two main classes of magnetic CVs. Polars have WDs that rotate ($P_{\rm spin}$) synchronously or near-synchronously with $P_{\rm orb}$ and Roche-Lobe-filling secondary star's rotation (M. Cropper 1990), whereas the intermediate polars (IPs) have asynchronous WDs, and most of them have $P_{\rm spin}/P_{\rm orb} \approx 0.01$–0.6 (J. Patterson 1994). The IPs evolve to shorter $P_{\rm orb}$; hence, its spin–orbital period ratio is expected to increase (e.g., A. J. Norton et al. 2008). Two subtypes of polars are the prepolars and low-accretion-rate polars (LARPs; A. D. Schwope et al. 2002, 2009). Both of them are synchronous systems. Historically, some objects now understood as prepolars were believed to be LARPs. Presently, these two types are considered to represent different evolutionary stages of a magnetic CV.

LARPs are polars that undergo prolonged low-accretion states in temporarily detached systems (e.g., L. Ferrario et al. 2015). On the other hand, prepolars are short $P_{\rm orb}$ systems (i.e., $P_{\rm orb} < 6$ hr) in which an M-type secondary star does not yet fill its Roche lobe but can show some accretion fed by the secondary's wind. Given recent discoveries of detached AR Sco–like systems, with magnetic WDs, prepolars can eventually evolve into polars (e.g., M. R. Schreiber et al. 2021).

In a seminal work, S. Tapia (1977) found that the linear polarization of AM Her, the polar prototype, varies with its $P_{\rm orb}$. Since then, many other polars showing variable linear and/or circular polarization were identified. The polarized emission from a magnetic CV is originated by cyclotron radiation produced in the so-called postshock region (PSR), and the variable polarization is the result of a changing view of the PSR (H. S. Stockman 1977). Cyclotron emission can also be established from the detection of cyclotron humps in the spectral continuum or spectropolarimetry. Polarization is usually high in polars (tens of percent). Some IPs (e.g., O. W. Butters et al. 2009) and prepolars (e.g., P. Hakala et al. 2022) exhibit small values of polarization, which is interpreted as a confirmation of magnetic accretion.

The exact classification of V1082 Sgr has not yet been settled. It was initially classified as a symbiotic system (D. Cieslinski et al. 1998), while J. R. Thorstensen et al. (2010) and F. Bernardini et al. (2013) argue in favor of a magnetic CV interpretation. G. Tovmassian et al. (2016, 2018a, 2018b) consider the classification as a detached system: it would be one of the first long-period prepolars, i.e., a prepolar with an early-K companion. However, X. Xu et al. (2019) proposed an evolutionary model in which V1082 Sgr is an IP with a Roche-lobe-filling K-type secondary.

No previous study has detected polarization in V1082 Sgr that would be an unquestionable evidence of a magnetic WD in the system and useful to disentangle its classification. Here, we report on the results of circular photopolarimetry of V1082 Sgr. We detected circular polarization in this system modulated with a period of 1.943 hr, which we interpret as the spin period, $P_{\rm spin}$, of the WD, characterizing it as a long-period IP. Section 2 describes the observations and data reduction. The results and the data analysis are shown in Section 3. Section 4 presents the modeling of the cyclotron emission of V1082 Sgr. The discussion and conclusions are presented in Sections 5 and 6, respectively.

2. Observation and Data Reduction

V1082 Sgr was observed for 10 nights spread over 2020 August and September using the 0.6 m Boller and Chivens telescope of the Observatório do Pico dos Dias operated by the Laboratório Nacional de Astrofísica, Brazil. Table 1 presents a summary of these observations. The polarimeter IAGPOL (A. M. Magalhães et al. 1996; C. V. Rodrigues et al. 1998) was configured with a quarter-wave retarder plate and a Savart plate. The observations were carried out using the CCD Ixon 4335, which has a pixel size of 13.5×13.5 μm. The plate scale is $0\farcs34$ pixel^{-1} in the previously mentioned instrumental setup.

All data sets were obtained in white light (i.e., no filters were used) in order to maximize the count rates. As pointed out by A. Bruch (2017), an estimate of the effective wavelength of the white light bandpass is 5530 Å, which is close to the effective wavelength of the Johnson V band (5500 Å). We therefore calibrate the V1082 Sgr magnitude using the star NOMAD

Table 1
Summary of the Observations

Date Obs.	Exp. Time (s)	Time Span (hr)	Mean mag (mag)
2020 Aug 22	200	4.5	14.0 ± 0.3
2020 Aug 23	120	6.2	14.2 ± 0.2
2020 Aug 24	120	5.6	14.1 ± 0.1
2020 Aug 25	120	5.9	14.2 ± 0.1
2020 Aug 26	100	6.1	14.1 ± 0.1
2020 Aug 27	130	2.8	13.9 ± 0.1
2020 Aug 30	150	6.1	14.2 ± 0.2
2020 Aug 31	150	5.7	13.7 ± 0.2
2020 Sep 1	150	2.6	14.2 ± 0.1
2020 Sep 2	150	6.1	14.5 ± 0.1

0692-0848091 ($\alpha_{2000.0} = 19^{\rm h}:07^{\rm m}:17\fs17$ and $\delta_{2000.0} = -20°:47':33\farcs02$), which has 13.9 mag in the V band (N. Zacharias et al. 2005). V1082 Sgr has an average V-band magnitude of 14.7 mag in NOMAD catalog.

The data reduction was performed using bias frames and dome calibration flat-field images to account for the detector's zero noise level and sensitivity. We also used polarized and unpolarized standard stars measurements to correct the linear polarization angle to the equatorial reference system and to verify the presence of spurious instrumental polarization. All procedures used the Image Reduction and Analysis Facility (IRAF)[15] and the PCCDPACK_INPE[16] (A. Pereyra et al. 2018; A. Pereyra 2000) packages. Tables A1 and A2 show the linear and circular polarization values of six standard stars from the southern hemisphere, observed on the same nights as V1082 Sgr. We confirmed that the instrumental circular polarization is negligible based on those values. The polarization was calculated from the ordinary and extraordinary ray fluxes ratio as described in C. V. Rodrigues et al. (1998). A correction for different efficiencies from ordinary and extraordinary counts was applied using a normalization factor as described by I. J. Lima et al. (2021). Each circular polarization point is calculated using differential flux measurements of a moving set of eight images gradually displaced across the time series. The circular polarization signal is not calibrated, i.e., the real signal of the circular polarization can be the inverse of the one presented here.

3. Results and Data Analysis

3.1. Photometry

The light curve of V1082 Sgr is shown in the upper panel of Figure 1. The system shows an average magnitude of 14.1 mag in the clear band calibrated to the V band as explained in Section 2. Table 1 shows the average magnitudes for each night. The photometric behavior of the system changed after the gap: the system shows a rapid brightness decline, then the system reaches its maximum flux in our observations, and then it evolves in a steady decline in the last nights (see Figure 1).

Our photometric data show no definite periods. The precise $P_{\rm orb}$ of the system (20.82 hr) was determined from the

[15] IRAF is distributed by the National Optical Astronomy, which is operated by the Association of Universities for Research in Astronomy, Inc., under a cooperative agreement with the National Science Foundation (D. Tody 1986, 1993).

[16] PCCDPACK_INPE can be downloaded from https://github.com/claudiavr/pccdpack_inpe/.

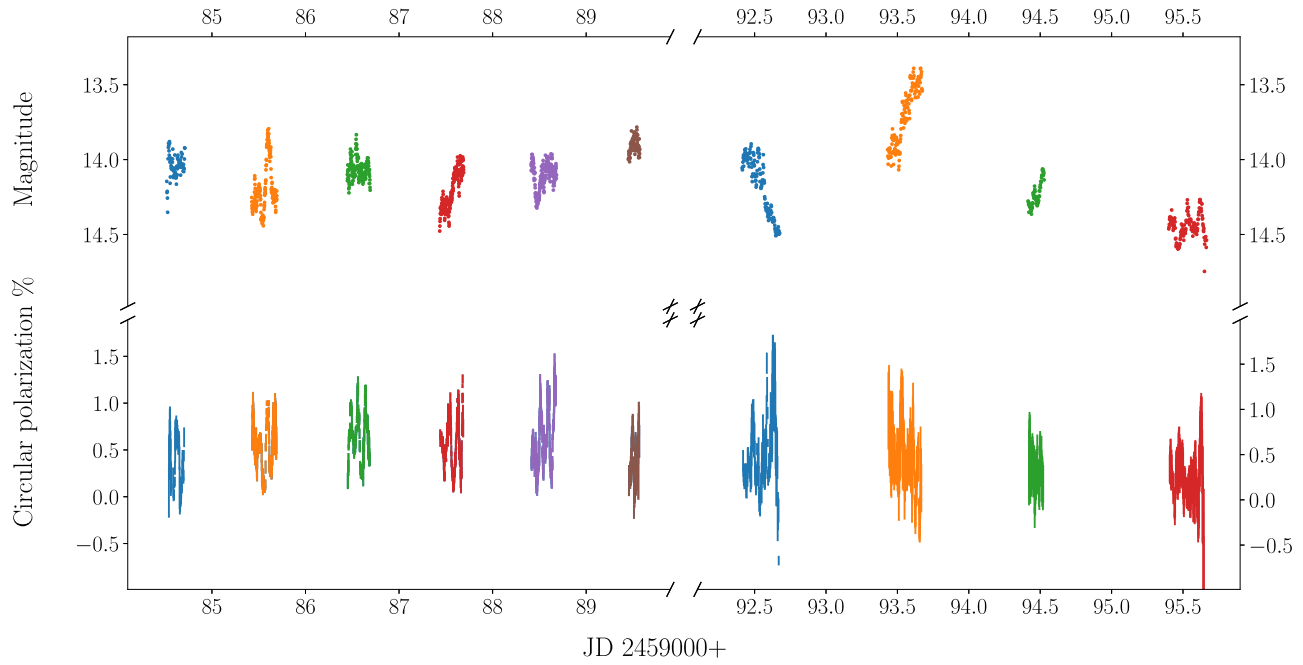

Figure 1. Photometry and circular polarimetry of V1082 Sgr over 10 nights of observations. The measurements were taken in the white band. The magnitude values were calibrated to the *V* band, as explained in Section 2.
(The data used to create this figure are available in the online article.)

spectroscopy (J. R. Thorstensen et al. 2010; G. Tovmassian et al. 2018a). $P_{\rm orb}$ was also detected in the photometric time series obtained by K2 mission (G. Tovmassian et al. 2018b) but only at a very low luminosity state during small fractions of the time. In the same 80 day long continuous monitoring of the system brightness by K2, there was no clear $P_{\rm spin}$ signal. G. Tovmassian et al. (2018b) noted a relatively significant peak at 11.2 cycles day^{-1} in the power spectrum, proposing it might be the optical counterpart of the frequency detected by F. Bernardini et al. (2013).

3.2. Polarimetry

The polarimetric observations of V1082 Sgr were obtained over 10 nights, which were divided into two blocks—Block A (first 6 nights) and Block B (last 4 nights)—separated by a gap of 2 nights. The small angular distance to the moon during observations in Block B caused the background to be higher; therefore Block A data have higher quality than Block B.

Our polarimetry is shown in the lower panel of Figure 1. The circular polarization degree measurements of V1082 Sgr are clearly variable in the range from −0.5% to 1.5%, but the individual points have larger errors. To search for periodicities, we calculated the power spectra of the circular polarization data using the Lomb–Scargle (LS; N. R. Lomb 1976; J. D. Scargle 1982) procedure, which was performed for the entire data set as well as separately for Blocks A and B (Figure 2). The power spectrum of Block A data shows a dominant peak at a frequency of 12.352 cycles day^{-1}, or a period of 0.081 day. We interpret this as the spin frequency of the WD in V1082 Sgr. In the case of Block B, there is a series of 1 day aliases peaking around ∼13 cycles day^{-1} (in both blocks, data were obtained nightly), consistent with the strongest peak found in Block A, while the highest power is located at the frequency of 1.154 cycles day^{-1}, corresponding to the orbital movement.

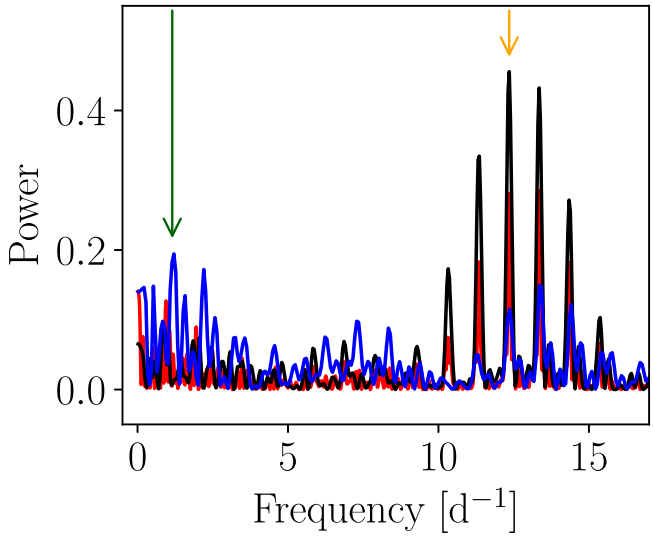

Figure 2. Power spectra of the circular polarization curves before detrending. The black line corresponds to the LS periodogram of Block A; the blue is for Block B, and the red corresponds to the entire data set. The vertical green arrow indicates the orbital frequency only detected in Block B. The spin frequency is marked with an orange arrow.

In Figure 3, we show the circular polarization degree curves for Blocks A (top) and B (bottom). The curves present a fast modulation (∼0.08 day) superposed on long-period trends. This ∼0.08 day period is obviously related to the peaks seen in the power spectra. The longer trends were modeled by sinusoidal functions whose frequencies were defined by the main low-frequency peak in each power spectrum, i.e., $f_2 = 0.185$ cycles day^{-1} for Block A (which roughly corresponds to the length of the block) and $f_2 = 1.154$ cycles day^{-1} for Block B. The sinusoidal fits (gray lines in Figure 3) were then subtracted to detrend the data.

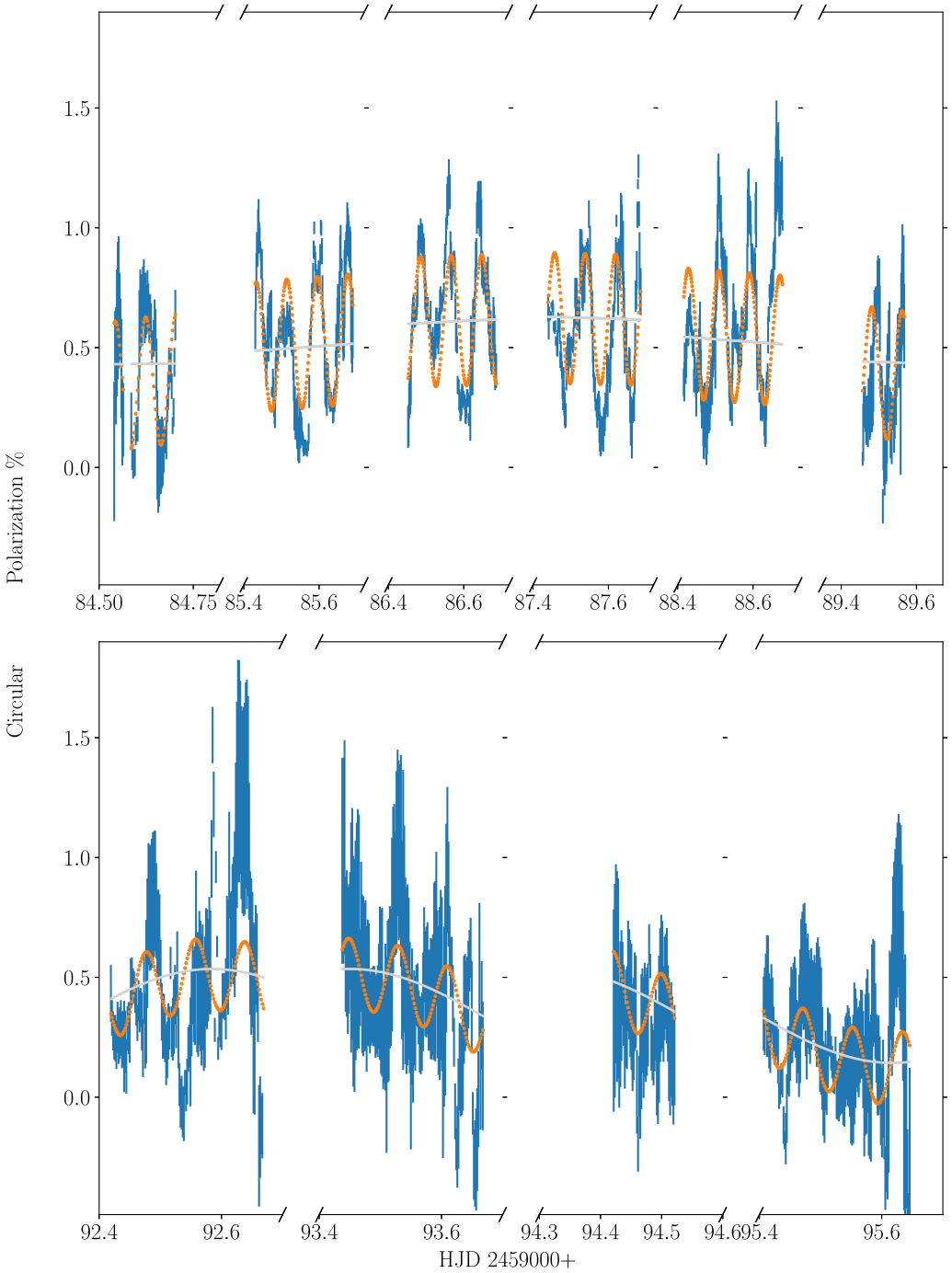

Figure 3. V1082 Sgr circular polarization observations for Block A (top panel) and Block B (lower panel). The blue line represents the data, with error bars, and the orange line is the fit with $P_{\rm spin} + f_2$, where f_2 is a low-frequency curve. In Block A, it roughly corresponds to the time length of Block A, and in Block B, $f_2 = P_{\rm orb}$. The f_2 curve is presented as a gray line.

The LS power spectra of the detrended data show the same peaks as the original data, especially the peak at frequency 12.352 cycles day^{-1}, or 1.943 hr. We supplemented the time series periodicity analysis with other methods such as the generalized LS, the discrete Fourier transform (DFT), the date-compensated DFT, and the phase dispersion minimization, all available in the software PERANSO (E. Paunzen & T. Vanmunster 2016). The periods obtained are all consistent with each other, pointing to $P = 0.08096 \pm 0.00005$ day ($=1.943 \pm 0.002$ hr), where the error is the standard deviation of the estimates using the different methods.

The phase diagram of the detrended circular polarization degree, folded at the 1.943 hr period and adopting T_0 from the spectroscopic stellar conjunction (G. Tovmassian et al. 2018a), is displayed in Figure 4, for each block. Both curves present one maximum and one minimum per cycle, and do not show changes in signal (the best-fitting sinusoids are always positive). However, there are differences in the amplitudes between the blocks, the amplitude in Block A being about twice that of Block B.

We explore the presence of $P_{\rm orb}$ in the circular polarization degree data from Block B. The polarization degree is the ratio

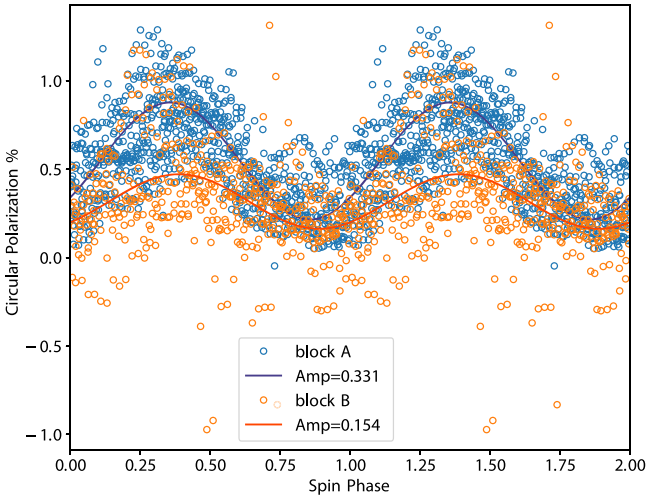

Figure 4. The circular polarization degree folded with the 1.943 hr P_{spin} of the magnetic WD in V1082 Sgr. Data in Blocks A and B are represented by blue and orange points, respectively. The values have been subtracted from long-term trends as explained in the text. The amplitudes are shown in the box. Phase zero corresponds to the spectroscopic orbital T_0.

between the polarized flux and the total flux, so it is affected by changes in the total flux that can come from different parts of the system. The circularly polarized flux, on the other hand, is an emission purely from the PSR. Within the uncertainties, the results of the timing analysis of the polarized flux and polarization degree in Block A are essentially the same. Block B data, however, do not show the P_{orb} modulation in the polarized flux, so we conclude that it is due to the total flux and it does not originate from the PSR. The P_{spin} is present in the polarized flux of Block B but with a smaller power than in Block A. Therefore, the consistent presence of the 1.943 hr period across both data segments, as well as in both the degree of polarization and the polarized flux, confirms that it represents the rotational period of a magnetic WD.

4. Modeling the Cyclotron Emission of V1082 Sgr

The polarized emission from magnetic CVs is due to the cyclotron radiation from the PSR. This region is located in the end of the magnetic accretion column near the magnetic poles of the WD. It is formed by the compression caused by a shock that occurs just above the WD surface. To estimate some properties of the PSR in V1082 Sgr, we performed a modeling of its circularly polarized flux. For that, we used the CYCLOPS code, which solves the radiative transfer in a 3D PSR (J. E. R. Costa & C. V. Rodrigues 2009; K. M. G. Silva et al. 2013; D. Belloni et al. 2021). The temperature and density profiles are consistently calculated considering the physical and geometric properties of the system as described in D. Belloni et al. (2021). Some model parameters are the WD mass, the mass-accretion rate, and the WD magnetic field, to cite the most relevant ones.

In the modeling, we use only Block A data. The input values to the model are circular polarized fluxes, which were obtained by multiplying the observed flux (in arbitrary units) by the circular polarization degree. No detrend was applied to the data. The result was then folded in 50 bins of spin phases. The total flux of V1082 Sgr is very variable, and it does not present any evidence of modulation with the P_{spin}, as found in the polarization. Therefore, we chose not to model the total flux

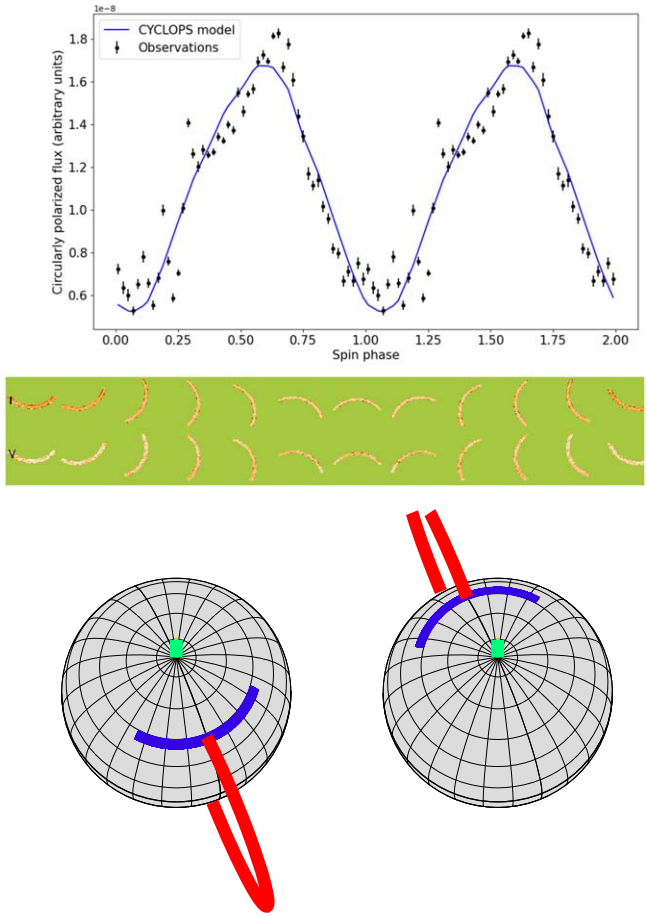

Figure 5. (Top) A model for the circularly polarized flux from the PSR of V1082 Sgr (blue line). Black points represent the observations. (Middle) 2D maps of the total intensity and circularly polarized flux in 12 spin phases separated by 30°. The flux scale increases from black to white, passing through orange. (Bottom) A projected view of the PSR region (in blue) over the WD surface in two phases of the WD rotation separated by half a cycle. The magnetic axis is shown as a green line, and the magnetic field line that crosses the center of the PSR is shown as a red line. See Section 4 for details of the model.

since the contribution from the PSR should be negligible compared with the emission from other system structures. On the other hand, the polarized flux comes only from the PSR and is a clean signal from this region. The emission was assumed monochromatic and calculated for a wavelength of 500 nm.

The top panel of Figure 5 presents the model superposed on V1082 Sgr observations. The model parameters are presented in Table 2. The reader can find a proper explanation of all parameters in J. E. R. Costa & C. V. Rodrigues (2009) and D. Belloni et al. (2021). The values of WD mass, the mass-accretion rate, and the inclination are considered fixed according to X. Xu et al. (2019), which provides the most updated estimates. Using the values of G. Tovmassian et al. (2018a) and F. Bernardini et al. (2013) to those parameters, we obtain a similar curve and the overall properties of the PSR are the same. For example, the magnetic field strength of the best-fit model changes to 9.4×10^6 G. The CYCLOPS code considers a centered dipolar magnetic field, whose axis can point to any direction. But, to minimize the number of free parameters, we adopted a magnetic axis parallel to the WD rotation axis. The model provides a WD magnetic field strength of approximately 10^7 G, a value within the standard range of IPs. The

Table 2
Parameters of the PSR of V1082 Sgr Modeled Using the CYCLOPS Code

Parameter	Value	Source
Fixed parameters		
Inclination	18°	X. Xu et al. (2019)
WD mass	0.77 $M_{\odot}$	X. Xu et al. (2019)
Mass-transfer rate	1.2×10^{-9} $M_{\odot}$ yr^{-1}	X. Xu et al. (2019)
Free parameters		
Angle between the center of the PSR and the WD rotations axis	44°	From the fit
Magnetic field in the magnetic pole	11×10^{6} G	From the fit
Longitudinal extension of the threading region	103°	From the fit
Radial extension of the threading region	0.16 $R_{\rm WD}$	From the fit
Some quantities obtained from the model		
Shock temperature	17.1 keV	Calculated from the model parameters
Threading radius	2.1 $R_{\rm WD}$	Calculated from the model parameters
PSR height	0.023 $R_{\rm WD}$	Calculated from the model parameters
Latitudinal extension of the PSR	4.°3	Calculated from the model parameters

Note. See text for details. $R_{\rm WD}$: WD radius.

temperature in the modeled PSR ranges from 1.2 to 17.1 keV at the base of the PSR and in the shock front, respectively. This is consistent with the fit of the XMM-Newton and Swift spectra presented by F. Bernardini et al. (2013), who use two MEKAL components of 0.12 keV and 13.2 keV. Using the same data but different modeling, X. Xu et al. (2019) estimated a $T_{\rm max}$ of 35^{+14}_{-9} keV, which is considerably larger than our results but barely consistent, considering the different approaches of the modeling.

In a dipolar magnetic geometry (as adopted by CYCLOPS), there can be two PSRs, each of them associated with one magnetic hemisphere. Our V1082 Sgr model adopts a single PSR region, and this does not imply any approximation because a possible second PSR associated with the magnetic pole pointing backward is always hidden from the observer view (see Figure 5, bottom panel). This is mainly a consequence of the small inclination of the system, but it also results from the angle between the WD rotation axis and the PSR. Therefore, a second PSR cannot contribute to the observed flux, even if two accretion columns exist.

To fit the observed shape of the polarized flux phase diagram, it is necessary to consider an azimuthally elongated PSR: the emission map of the PSR is presented in the middle panel of Figure 5. As the PSR footprint reflects the threading region (i.e., the region in the equatorial plane from where the accretion flow begins to follow the WD magnetic field lines) geometry, the coupling of the flux with the magnetic field lines should occur along an extended region in the equatorial plane. Moreover, this PSR is observable in all spin phases, so no modulation due to self-eclipse by the WD is possible in this model. The changing view of the PSR causes the variation of the optical circular polarization, since the cyclotron emission depends on the angle between the magnetic field and the observer.

The CYCLOPS code considers the entire geometry of the magnetic accretion column. In particular, the model geometry is built from the threading region. Our model leads to a threading region located at 2.1 WD radii ($R_{\rm WD}$) from the WD surface. Using the model parameters, the magnetospheric radius of V1082 Sgr is 3.2 $R_{\rm WD}$ (considering the expression of L. Ferrario et al. 1989), which is similar to the threading region value of our model providing a consistent picture of the system configuration.

5. Discussion

G. Tovmassian et al. (2016, 2018a, 2018b) argued that V1082 Sgr could be a prepolar. The arguments in favor of the prepolar hypothesis for V1082 Sgr are the very long $P_{\rm orb}$, at which it is difficult to form a Roche-lobe-filling CV with a K-type secondary, and the very irregular, fast variability, associated with the changing accretion rate. The counter-argument is that even a fast-rotating, magnetically active K-star could hardly provide stellar winds of the order of 10^{-9}–10^{-10} $M_{\odot}$ yr^{-1} needed to explain the high luminosity, larger than 10^{34} erg s^{-1}, of V1082 Sgr. X. Xu et al. (2019) proposed an alternative scenario in which the system underwent a thermal timescale mass-transfer episode in the past and currently is a Roche-lobe-filling IP with a low-mass secondary, which, however, has a temperature corresponding to an early K-type star. The circular polarization in magnetic CVs comes from a structure anchored on the WD, so the period of 1.943 hr found in V1082 Sgr is certainly the WD $P_{\rm spin}$. It rules out a polar or a prepolar classification since these are synchronous systems. Therefore, V1082 Sgr should be a long-orbital-period IP in line with the scenario proposed by X. Xu et al. (2019).

Unlike the polars, which have large and ubiquitous circular polarization levels of several tens of percent (e.g., A. S. Oliveira et al. 2019), IPs have low-level circular polarization or even nondetected polarized flux. For example, V2731 Oph (O. W. Butters et al. 2009) is one of the most polarized IPs: the spin-folded circular polarization curve shows a peak-to-peak amplitude of 8.26 ± 1.56% in the B band (and about 3% in the U, V, R, and I bands). For V1082 Sgr, we found an amplitude for the circular polarization of around 1.0%, in agreement with typical values found in other IPs.

V1082 Sgr has $P_{\rm spin}/P_{\rm orb}$ equal to 0.093, which is a typical value for an IP (A. R. King & J.-P. Lasota 1991; K. Mukai 2017). Moreover, that $P_{\rm spin}$ makes V1082 Sgr the IP with the third-longest $P_{\rm spin}$, after RX J2015.6+3711 (F. Coti Zelati et al. 2016) and Paloma (R. Schwarz et al. 2007; A. Joshi et al. 2016;

Table 3
IPs with P_{orb} Longer than ∼10 hr

Object	P_{orb} (hr)	P_{spin} (hr)	P_{spin}/P_{orb} (hr)	Circular Polarization; Reference (%)
GK Per	47.92	0.097	0.002	+0.03 ± 0.10; (1)
V1082 Sgr	20.82	1.943 (2)	0.093	0 to 1; (2)
Swift J2006.4+3645	17.28	0.048	0.003	⋯
V2731 Oph	15.42	0.035	0.002	−4 to +4.26; (3)
IGR J17014-4306	12.82	0.516	0.040	0 to −2.5; (4)
RX J2015.6+3711	12.76	1.998	0.156	⋯
V1062 Tau	9.98	1.056	0.106	⋯

Note. The values of P_{orb} and P_{spin} are from the Mukai's IP Homepage and references therein.
References. (1) H. S. Stockman et al. (1992), reported the mean value; (2) this paper; (3) O. W. Butters et al. (2009), for *B* band; (4) S. B. Potter & D. A. H. Buckley (2018).

J. R. Thorstensen et al. 2017; C. Littlefield et al. 2023) with 2 hr and 2.27 hr, respectively. Paloma has a value of P_{spin}/P_{orb} larger than 0.85, which is very odd for an IP. It is a member of a (new) group of several magnetic CVs whose WDs rotate with frequencies around 90% of the orbital one (K. G. Pradeep et al. 2024). On the other hand, RX J2015.6+3711 is also a long orbital-period IP, with a period of around 12.76 hr (J. P. Halpern et al. 2018). Table 3 enumerates the IPs having the longest ($\gtrsim$10 hr) P_{orb}. Figure 6 shows the distribution of currently confirmed IPs in the P_{spin}-versus-P_{orb} plane from Mukai's Intermediate Polars Homepage.[17] We added to this plot the location of V1082 Sgr, which is close to the $P_{spin} = 0.1 \times P_{orb}$ line and in the upper right limit of this distribution. We also highlighted in this plot other long orbital-period IPs.

The accretion mode/geometry of IPs is an old and complex subject (see, for instance, C. Hellier 1991). A. J. Norton et al. (2004, 2008) shed some light on this topic through simulations of accretion onto magnetic WDs. These studies showed numerically that P_{spin}/P_{orb} can be used to unravel the accretion modes of IPs. We can have a hint of whether V1082 Sgr is in spin equilibrium, understood as the balance of angular momentum in the accretion process, by checking its position in Figure 2 of A. J. Norton et al. (2004). This figure shows the results of simulations for P_{orb} from 80 minutes to 10 hr, so some extrapolation should be considered for $P_{orb} = 20$ hr: the model line for such a period should be to the right of the models lines depicted in the figure. Considering a magnetic moment of 4.3×10^{33} G cm^3, V1082 Sgr would be placed above the spin equilibrium line. In case it is true, the WD should be in a spin-up state, i.e., evolving to shorter P_{spin} to achieve the spin equilibrium. The corotation radius, R_{co}, of V1082 Sgr for a Keplerian period P_{spin} is 69 R_{WD}. R_{co} is not exactly the equilibrium radius for the magnetic accretion, but they are assumed to be similar (see A. J. Norton et al. 2004, and references therein). The circularization radius, R_{circ}, of V1082 Sgr is around 40 R_{WD}, so much smaller than the R_{co}. These numbers are consistent with V1082 Sgr not being a synchronous system, a situation in which R_{mag} should also be larger or around R_{circ}. Our estimate of R_{mag} is approximately 3 R_{WD}, which is consistent with this scenario. Moreover, the huge difference between R_{mag} and R_{co} also points to a system out of equilibrium.

An evaluation of the accretion geometry of V1082 Sgr can be done based on the results of A. J. Norton et al. (2008). Their Figure 2 illustrates the possible accretion structures for an asynchronous magnetic CV as a function of P_{spin} and magnetic field for $P_{orb} = 4$ hr and a mass ratio ($q = M_2/M_1$) equal to 0.5. The central panel of this figure shows that the stream-like accretion can occur for any value of magnetic moment. In particular, a stream-like geometry (i.e., with no disk at all—top left panel of that figure) can occur for small values of the magnetic field if P_{spin} is long enough. In this case, the threading region is located near the WD. To verify if this could be the case for V1082 Sgr, we should inspect A. J. Norton et al.'s (2008) Figure 5. For $q = 0.5$, values of $P_{spin}/P_{orb} \lesssim 0.1$ correspond to disklike accretion. V1082 Sgr has P_{spin}/P_{orb} ratio of 0.093 and an estimated mass ratio of around 0.7 (X. Xu et al. 2019): this mass ratio decreases the aforementioned limit. So this system would be in the limit between a disklike and stream-fed accretion. Therefore, we could suppose that V1082 Sgr is located in a region where stream accretion is possible. A stream geometry is more prone to strong changes in the accretion states because there is no disk to act as a material reservoir. For example, the substantial alterations in brightness observed in polars are likely due to this phenomenon. Therefore, it is possible that the variability of the accretion rates of V1082 Sgr is related to the absence of an accretion disk in the system. Moreover, a stream-like geometry is consistent with a spin-up WD (A. J. Norton et al. 2008), as discussed in the previous paragraph. However, the conclusion that

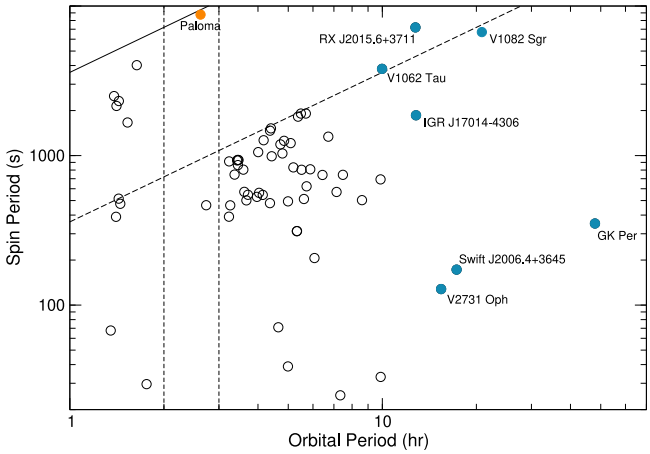

Figure 6. P_{spin} vs. P_{orb} for IPs. V1082 Sgr and other long P_{orb} objects discussed in the text are highlighted in blue, while the nearly synchronous, short P_{orb} IP Paloma is depicted in orange. The vertical lines are the period gap interval of 2–3 hr, and the diagonal lines represent $P_{spin} = P_{orb}$ (solid) and $P_{spin} = 0.1 \times P_{orb}$ (dashed). Data, except for V1082 Sgr, are from Mukai's IP Homepage (see text).

[17] https://asd.gsfc.nasa.gov/Koji.Mukai/iphome/iphome.html

V1082 Sgr is a stream-fed system should be taken with a grain of salt because q can be as small as 0.25 (G. Tovmassian et al. 2025, in preparation), placing V1082 Sgr in the disk-accretion region.

F. Bernardini et al. (2013) reported an extensive study of X-ray data of V1082 Sgr obtained with XMM-Newton, Suzaku, and Swift from 2008 until 2012. The light curve of XMM-Newton-PN data, with energies ranging between 0.3 and 15 keV, shows a modulation with a period of about 2 hr, which was only present during some observation intervals. This modulation is energy dependent, with a pulsed fraction decreasing toward higher energies. A similar, ∼2 hr modulation was also detected during a Suzaku observation and less significantly during Swift pointings. This 2 hr modulation was not persistent, so it was interpreted as due to noncoherent transient accretion.

We argue that the intermittent 2 hr modulation seen in X-rays is also related to the WD spin. Important radiative cooling processes in the PSR of magnetic CVs are the cyclotron emission, responsible for the optical polarization, and bremsstrahlung, which contributes with an important fraction of X-ray emission. While the cyclotron emission is intrinsically anisotropic and, therefore, can be modulated with the WD $P_{\rm spin}$, the bremsstrahlung emission is usually optically thin and isotropic, so there should be external mechanisms to produce flux variability. In magnetic CVs in general and in IPs in particular, the modulation of the X-ray emission can be produced by the self-occultation of PSR by the WD or by phase-dependent absorption/scattering of the PSR emission by structures lying between the PSR and the observer, as the upper portion of the magnetic column (A. J. Norton 1993; D. Belloni et al. 2021). Self-occultation is a geometric effect and does not depend on energy. On the other hand, photoelectric absorption depends on energy, decreasing from soft to hard X-rays, consistent with the pulsed-fraction energy dependence reported by F. Bernardini et al. (2013). Moreover, the inclination of V1082 Sgr and the proposed location of its PSR prevent any modulation due to self-eclipse. However, the intermittence of the X-ray modulation remains to be explained. It could be connected with the extreme variation of the accretion rate, which can occasionally drop to negligible values in V1082 Sgr (G. Tovmassian et al. 2016). The accretion rate affects not only the density of the PSR itself but also the density of the "upper" structures responsible for the absorption. In particular, a stream-accretion geometry is more susceptible to reflect the mass-accretion variations.

6. Conclusions

We have detected a periodicity of 1.943 ± 0.002 hr in the circular polarization of V1082 Sgr, with an amplitude smaller than 1%. We interpret this period as the rotation of a magnetic WD, since the polarized flux is produced by cyclotron emission from the PR near the WD surface. This indicates that V1082 Sgr is an IP, in agreement with the suggestion of X. Xu et al. (2019). Also, the intermittent period near 2 hr found in X-ray data by F. Bernardini et al. (2013) is possibly related to the WD spin and could be associated with phase-dependent absorption structures in the accretion column.

The CYCLOPS model of the cyclotron emission of V1082 Sgr yields a magnetic field strength of 10^7 G and temperatures that vary from 17 keV in the top of the PSR to 1 keV in the bottom, in line with X-ray determinations by F. Bernardini et al. (2013). According to the model, the threading region is placed at a distance of 2.1 $R_{\rm WD}$ from the WD surface, roughly at a similar position to the estimated magnetospheric radius. Considerations about this radius and the expected corotation radius indicate that V1082 Sgr is out of spin equilibrium. This conclusion is reinforced by a comparison of the values of the $P_{\rm spin}/P_{\rm orb}$ ratio and the estimated magnetic moment with published simulations, which indicate that the WD is in a spin-up state. In spite of the reasonable CYCLOPS fitting, more restrictive modeling of the PSR should be based on multiband emission since the cyclotron emission is highly dependent on the frequency. The $P_{\rm spin}$-versus-$P_{\rm orb}$ relation also points to a possible stream-accretion mode on V1082 Sgr, which in turn could be associated with the recorded highly variable optical brightness states and intermittent X-ray periodic modulation due to the absence of a disk as a mass reservoir.

V1082 Sgr is, therefore, the known IP with the second-longest $P_{\rm orb}$ and with the third-longest $P_{\rm spin}$, which places it as an important case to the understanding of the evolution of magnetic CVs. We foresee many additional studies for this system, for instance, an observational verification of the WD spin-up; a better constrained model for its PSR; and Doppler tomography to better define the accretion geometry.

Acknowledgments

I.J.L. acknowledges support from grant ANPCYT-PICT 0901/2017 (Argentina) and Coordenação de Aperfeiçoamento de Pessoal de Nìvel Superior—Brazil (CAPES, number #88887.913793/2023-00). G.T. was supported by grants IN109723 and IN110619 from the Programa de Apoyo a Proyectos de Investigación e Innovación Tecnológica (PAPIIT). This research was supported in part by grant NSF PHY-1748958 to the Kavli Institute for Theoretical Physics (KITP). C.V.R. thanks the Brazilian Ministry of Science, Technology and Innovation (MCTI) and the Brazilian Space Agency (AEB) by the support through the PO 20VB.0009 and also the Conselho Nacional de Desenvolvimento Cientìfico e Tecnológico (CNPq grant: 310930/2021-9). This research was supported in part by the National Science Foundation under grant No. NSF PHY-1748958 (CVR). A.S.O. acknowledges São Paulo Research Foundation (FAPESP) for financial support under grant #2017/20309-7. G.J.M.L. is member of the CIC-CONICET (Argentina). A.C.M. thanks the CNPq (Proc: #150737/2024-6). DCS thanks the CAPES (Proc: #88887.714650/2022-00 and #88881.846501/2023-01). W.S. thanks the CNPq (Proc: #318052/2021-0, #300343/2022-1, #300834/2023-3, #301366/2023-3, #300252/2024-2 and #301472/2024-6). F.F. thanks the CNPq (Proc: #141350/2023-7).

Facility: LNA:BC0.6m.

Software: IRAF (D. Tody 1986, 1993), PCCDPACK_INPE (A. Pereyra et al. 2018; A. Pereyra 2000), PERANSO (E. Paunzen & T. Vanmunster 2016).

Appendix
Observations of Polarimetric Standard Stars

In this appendix, we present a summary of the measurements of polarimetric standard stars obtained in the same observational run of V1082 Sgr. Table A1 shows the average linear and circular polarizations of linearly polarized stars. The position-angle values are not calibrated to the equatorial system. The

Table A1
Average Polarization Measurements of Linearly Polarized Standard Stars

Object	P_l (%)	PA (deg)	P_C (%)	Number of Observations
HD 161056	3.64 ± 0.11	46.6	0.08 ± 0.07	6
Hilt 785	4.08 ± 0.05	154.2	0.03 ± 0.03	5
Hilt 781	3.81 ± 0.05	152.3	0.02 ± 0.03	6

Note. Pl is the linear polarization; PA is the polarization angle; PC is the circular polarization.

Table A2
Average Polarization Measurements of Unpolarized Standard Stars

Object	P_l (%)	P_C (%)	Number of Observations
WD 2007-303	0.10 ± 0.11	0.12 ± 0.17	4
WD 2149+021	0.13 ± 0.19	0.07 ± 0.11	2
WD 2039-202	2.22 ± 0.56	0.09 ± 0.44	2

circular polarization values are consistent with zero. Table A2 shows the results for unpolarized stars. Again, the values of circular polarization are consistent with zero. These results demonstrate that our measurements are not affected by instrumental circular polarization in a level of 0.1% or smaller.

ORCID iDs

I. J. Lima https://orcid.org/0000-0001-6013-1772
G. Tovmassian https://orcid.org/0000-0002-2953-7528
C. V. Rodrigues https://orcid.org/0000-0002-9459-043X
A. S. Oliveira https://orcid.org/0000-0001-6422-9486
G. J. M. Luna https://orcid.org/0000-0002-2647-4373
D. A. H. Buckley https://orcid.org/0000-0002-7004-9956
K. M. G. Silva https://orcid.org/0000-0003-1949-4621
A. C. Mattiuci https://orcid.org/0000-0002-0337-1363
D. C. Souza https://orcid.org/0000-0001-9255-864X
W. Schlindwein https://orcid.org/0000-0002-7095-4147
F. Falkenberg https://orcid.org/0000-0002-8646-218X
M. S. Palhares https://orcid.org/0000-0002-0396-8725

References

Belloni, D., Rodrigues, C. V., Schreiber, M. R., et al. 2021, ApJS, 256, 45
Bernardini, F., de Martino, D., Mukai, K., et al. 2013, MNRAS, 435, 2822
Bruch, A. 2017, NewA, 52, 112
Butters, O. W., Katajainen, S., Norton, A. J., Lehto, H. J., & Piirola, V. 2009, A&A, 496, 891
Cieslinski, D., Steiner, J. E., & Jablonski, F. J. 1998, A&AS, 131, 119
Costa, J. E. R., & Rodrigues, C. V. 2009, MNRAS, 398, 240
Coti Zelati, F., Rea, N., Campana, S., et al. 2016, MNRAS, 456, 1913
Cropper, M. 1990, SSRv, 54, 195
Ferrario, L., de Martino, D., & Gansicke, B. T. 2015, SSRv, 191, 111
Ferrario, L., Wickramasinghe, D. T., & Tuohy, I. R. 1989, ApJ, 341, 327
Hakala, P., Parsons, S. G., Marsh, T. R., et al. 2022, MNRAS, 513, 3858
Halpern, J. P., Thorstensen, J. R., Cho, P., et al. 2018, AJ, 155, 247
Hellier, C. 1991, MNRAS, 251, 693
Joshi, A., Pandey, J. C., Singh, K. P., & Agrawal, P. C. 2016, ApJ, 830, 56
King, A. R., & Lasota, J.-P. 1991, ApJ, 378, 674
Lima, I. J., Rodrigues, C. V., Ferreira Lopes, C. E., et al. 2021, AJ, 161, 225
Littlefield, C., Hoard, D. W., Garnavich, P., et al. 2023, AJ, 165, 43
Lomb, N. R. 1976, Ap&SS, 39, 447
Magalhães, A. M., Rodrigues, C. V., Margoniner, V. E., Pereyra, A., & Heathcote, S. 1996, in ASP Conf. Ser. 97, Polarimetry of the Interstellar Medium, ed. W. G. Roberge & D. C. B. Whittet (San Francisco, CA: ASP), 118
Mukai, K. 2017, PASP, 129, 062001
Norton, A. J. 1993, MNRAS, 265, 316
Norton, A. J., Butters, O. W., Parker, T. L., & Wynn, G. A. 2008, ApJ, 672, 524
Norton, A. J., Wynn, G. A., & Somerscales, R. V. 2004, ApJ, 614, 349
Oliveira, A. S., Rodrigues, C. V., Palhares, M. S., et al. 2019, MNRAS, 489, 4032
Patterson, J. 1994, PASP, 106, 209
Paunzen, E., & Vanmunster, T. 2016, AN, 337, 239
Pereyra, A. 2000, Phd thesis, Instituto Astronômico e Geofísico, Universidade de São Paulo
Pereyra, A., Magalhães, A. M., Rodrigues, C., & Carciofi, A. 2018, PCCDPACK: Polarimetry with CCD, Astrophysics Source Code Library, ascl:1809.002
Potter, S. B., & Buckley, D. A. H. 2018, MNRAS, 473, 4692
Pradeep, K. G., Singh, K. P., Dewangan, G. C., et al. 2024, MNRAS, 527, 774
Rodrigues, C. V., Cieslinski, D., & Steiner, J. E. 1998, A&A, 335, 979
Scargle, J. D. 1982, ApJ, 263, 835
Schreiber, M. R., Belloni, D., Gänsicke, B. T., Parsons, S. G., & Zorotovic, M. 2021, NatAs, 5, 648
Schwarz, R., Schwope, A. D., Staude, A., et al. 2007, A&A, 473, 511
Schwope, A. D., Brunner, H., Hambaryan, V., & Schwarz, R. 2002, in ASP Conf. Ser. 261, The Physics of Cataclysmic Variables and Related Objects, ed. B. T. Gänsicke, K. Beuermann, & K. Reinsch (San Francisco, CA: ASP), 102
Schwope, A. D., Nebot Gomez-Moran, A., Schreiber, M. R., & Gänsicke, B. T. 2009, A&A, 500, 867
Silva, K. M. G., Rodrigues, C. V., Costa, J. E. R., et al. 2013, MNRAS, 432, 1587
Stockman, H. S. 1977, ApJL, 218, L57
Stockman, H. S., Schmidt, G. D., Berriman, G., et al. 1992, ApJ, 401, 628
Tapia, S. 1977, ApJL, 212, L125
Thorstensen, J. R., Peters, C. S., & Skinner, J. N. 2010, PASP, 122, 1285
Thorstensen, J. R., Ringwald, F. A., Taylor, C. J., et al. 2017, RNAAS, 1, 29
Tody, D. 1986, Proc. SPIE, 627, 733
Tody, D. 1993, in ASP Conf. Ser. 52, Astronomical Data Analysis Software and Systems II, ed. R. J. Hanisch, R. J. V. Brissenden, & J. Barnes (San Francisco, CA: ASP), 173
Tovmassian, G., González, J. F., Hernández, M. S., et al. 2018a, ApJ, 869, 22
Tovmassian, G., González-Buitrago, D., Zharikov, S., et al. 2016, ApJ, 819, 75
Tovmassian, G., Szkody, P., Yarza, R., & Kennedy, M. 2018b, ApJ, 863, 47
Tueller, J., Baumgartner, W. H., Markwardt, C. B., et al. 2010, ApJS, 186, 378
Xu, X., Shao, Y., & Li, X.-D. 2019, MNRAS, 489, 3031
Zacharias, N., Monet, D. G., Levine, S. E., et al. 2005, yCat, 1297, 0